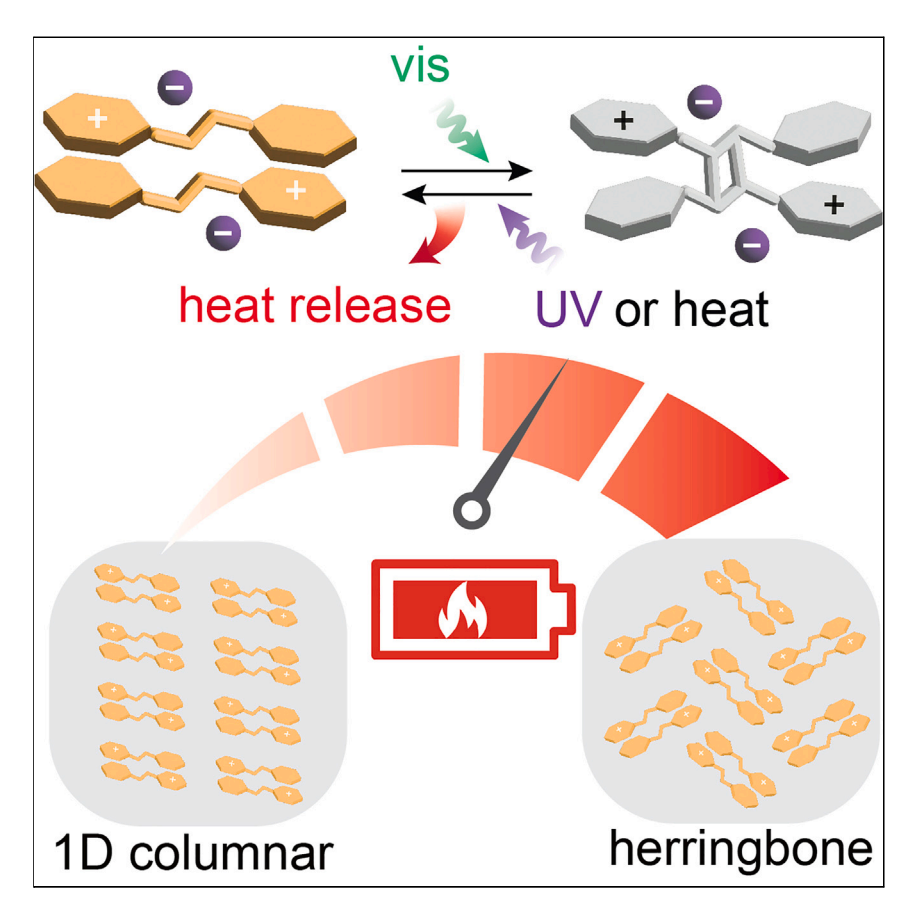




Article

Solid-state photon energy storage via reversible [2+2] cycloaddition of donor-acceptor styrylpyrylium system



The [2+2] intermolecular photocycloaddition of styrylpyrylium was investigated for molecular solar thermal (MOST) energy storage, which enables storing solar photon energy and releasing heat on demand. The molecular system displays desired properties, including visible light absorption, long-term energy storage, and excellent cyclability. Furthermore, the impact of molecular packing in crystals on the MOST energy storage density is revealed through the elucidation of crystal structures of compounds.

Sungwon Cho, Junichi Usuba, Subhayan Chakraborty, Xiang Li, Grace G.D. Han

gracehan@brandeis.edu

Highlights

Styrylpyrylium derivatives that undergo [2+2] photocycloaddition are reported

Long-term solid-state energy storage through visible light activation is achieved

This provides insights for designing solid-state materials for solar energy storage



Cho et al., Chem 9, 1–13 November 9, 2023 © 2023 Elsevier Inc. https://doi.org/10.1016/j.chempr.2023.06.007

Chem



Article

Solid-state photon energy storage via reversible [2+2] cycloaddition of donor-acceptor styrylpyrylium system

Sungwon Cho, ¹ Junichi Usuba, ¹ Subhayan Chakraborty, ^{1,2} Xiang Li, ^{1,2} and Grace G.D. Han^{1,3,*}

SUMMARY

Donor-acceptor styrylpyrylium derivatives are reported to absorb visible light to undergo intermolecular [2+2] cycloaddition to form cyclobutane structures in crystal, storing up to 42 kJ/mol of energy in strained chemical bonds with half-lives as long as 32 years. The reversion is triggered either by UV irradiation or thermal activation to release the energy, and the solid-state energy storage-release process is repeated without decomposition for over 10 cycles. By varying functional groups on the donor moiety and counter-anions, we fine-tuned the 3D packing in crystals and electrostatic interactions between the cationic molecules and anions, which primarily determine the energy storage capacity of the compounds. This quantitative and mechanistic study on the energy storage capability of styrylpyryliums, supported by an in-depth crystal structure analysis as well as optical and thermal property measurements, will shed light on the development of new molecular solar thermal energy storage materials with highly desired properties beyond conventional photoswitches.

INTRODUCTION

A variety of photoswitches including azo(hetero)arenes, 1-5 hydrazones, 6 norbornadiene (NBD)/quadricyclane (QC) couples, 7.8 and dihydroazulene (DHA)/vinylheptafulvene (VHF) systems 9.10 have been reported to absorb solar photons to isomerize from the thermodynamically stable state to a metastable state and store energy in strained chemical bonds. These molecular solar thermal (MOST) energy storage compounds release the stored energy as heat upon the triggered structural reversion to the thermodynamically stable state. 11.12 For MOST systems, absorption wavelengths of light, photo-conversion yields at photostationary states, reversibility of isomerization, half-lives of metastable isomers, and relative energy level of thermodynamically stable and metastable states are the primary figures of merit that determine their energy conversion efficiency, energy storage time, and energy storage density. Various functionalization strategies have been developed for each class of photoswitches to optimize the performance of MOST systems, and some of the desired properties have been successfully achieved.

The photoswitches generally undergo large structural changes during reversible isomerization, particularly during *E-Z* isomerization^{13,14} and ring opening-closing process, ^{15,16} which are easily monitored in dilute solutions. However, the photoswitching processes are often challenging to achieve in condensed phases, especially in the solid state, due to the limited conformational freedom of photoswitches in a packed environment, which hinders their structural changes.¹⁷ The ability to

THE BIGGER PICTURE

Photoswitches are capable of storing and releasing energy through photon absorption of different wavelengths for molecular solar thermal energy storage applications. However, many of the well-studied photoswitches primarily absorb UV, which comprises only about 4% of the solar spectrum. The switching also requires either the dissolution of the compounds or phase change to the liquid phase that introduces combustible organic fluids to the energy storage system. Therefore, a series of styrylpyrylium derivatives that undergo visible light-induced [2+2] photocycloaddition to strained cyclobutane structures are developed to realize a longterm energy storage system in the solid state, which also harnesses the broad spectrum of sunlight. This work overcomes the critical challenges of conventional photoswitches and demonstrates photochemical reactions in solid state for solar energy storage applications.





store and release energy in condensed phases is important for accomplishing MOST applications with large gravimetric and volumetric energy densities since the dissolution of switches in solvent drastically lowers the energy density of the system. Although a range of strategies including the encapsulation of switches in metalorganic frameworks or cages have successfully improved the yield of solid-state isomerization, ^{18–20} the presence of encapsulation materials lowers the energy density of the system. Therefore, the functionalization of photochromes with groups that decrease the intermolecular interactions among them in a close-packed environment has been developed. Such functionalized photoswitches, e.g., azo(hetero)arenes^{21,22} and hydrazones, ⁶ undergo solid-state photoisomerization, and as a result of their significant structural and polarity changes, the metastable-state isomers often form a liquid phase. The photo-induced solid-to-liquid phase transition has been utilized as an effective method that enhances the overall energy storage density of MOST compounds, but the presence of the liquid phase poses a challenge of potential leakage and risk of combustion in applications.²³

Herein, we report a series of donor-acceptor styrylpyrylium (STP) compounds that undergo photo-induced intermolecular [2+2] cycloaddition to cyclobutane (CB) in a crystalline state, which then reverts to STP to release substantial energy. Beyond the intramolecular [2+2] cycloaddition of NBD, the photochemical [2+2] or [4+4] reactions have been rarely explored for successful MOST applications due to the facile photo-induced oxidation that produces phenanthrene from stilbene and anthraguinone from anthracene. 24-26 The potential of the donor-acceptor STP/ CB system for reversible cycloaddition and energy storage was first probed by Hesse and Hünig in 1985, who reported qualitative thermal reversion of two CB derivatives at 148°C and 101°C.²⁷ However, the quantity of stored energy, energy storage time in CB, photochemical reversion and energy release, or impact of counter-anions and functionalization patterns on the energy storage-release process were not investigated. Another report by Novak et al. in 1993 also only describes the photo-induced single-crystal-to-single-crystal conversion of STP to CB without any analysis of their potential as reversible energy storage materials.²⁸ Thus, there exists a critical need to unravel this solid-state [2+2] cycloaddition and reversion process and develop design principles for the STP/CB system that achieve facile conversion of solar photons in the visible light range, large energy storage densities, long energy storage time, and efficient energy release upon triggering.

RESULTS AND DISCUSSION

The STP/CB system is now revealed as a new class of MOST compounds with substantial energy storage densities (vide infra), similar to that of pristine azobenzene (41 kJ/mol). The mechanism of solar photon energy storage is illustrated in Figure 1A. The head-to-tail assembly of STP in crystalline solid, facilitated by the intermolecular π -interactions between an electron-rich phenyl group and an electron-deficient pyrylium moiety, enables the photo-induced [2+2] cycloaddition of two STP molecules to form a CB product. One of the unique features of STP systems is its broad visible light absorption in the solid state (typical range of 400–600 nm), which induces [2+2] cycloaddition (Figure 1B). This is in contrast to other [2+2] or [4+4] cycloaddition-based MOST compounds including NBD/QC couples and anthracenes that report a maximum λ_{onset} of $\sim\!450$ nm. 30,31 The push-pull structure of STP, functionalized with the electron-donating group(s) on the phenyl ring and bearing an electron-deficient pyrylium, displays a red-shifted absorption profile compared with stilbenes or stilbazoles without the push-pull design. $^{32-34}$ The

¹Department of Chemistry, Brandeis University, Waltham, MA 02453, USA

²These authors contributed equally

³Lead contact

^{*}Correspondence: gracehan@brandeis.edu https://doi.org/10.1016/j.chempr.2023.06.007





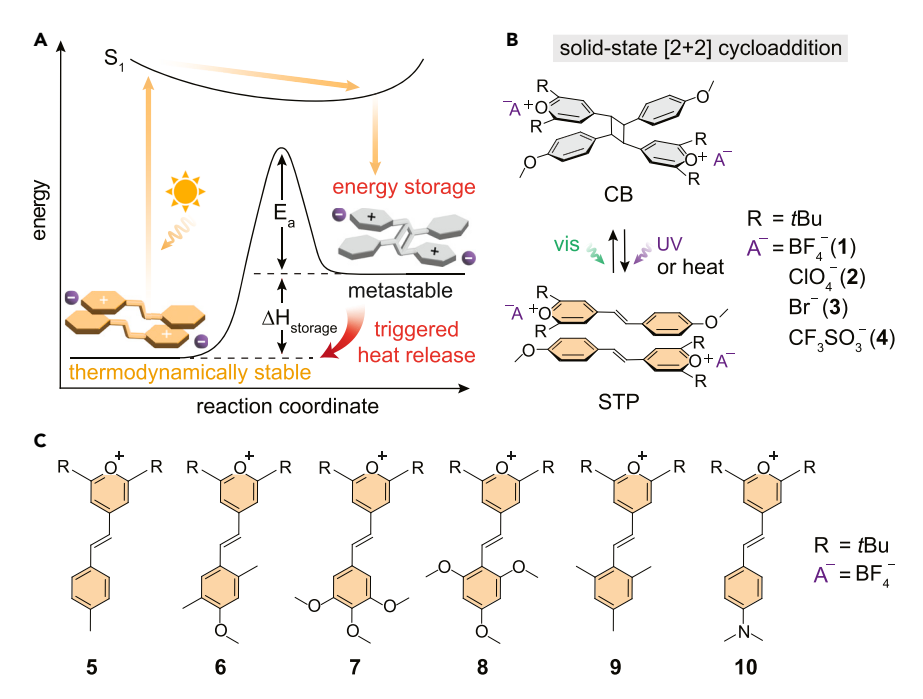


Figure 1. Energy storage concept and chemical structures of styrylpyryliums

(A) An energy diagram illustrating solar photon energy storage through [2+2] cycloaddition and energy release by triggered cycloreversion.

(B) Reversible photo-induced [2+2] cycloaddition and reversion between styrylpyrylium (STP) and cyclobutane (CB) with varied counter-anions (A^-).

(C) Chemical structures of STP derivatives with varied functional groups on the phenyl ring.

absorption of visible light instead of UV is an attractive characteristic for MOST applications that aim to harness a large portion of the solar spectrum.

The CB cycloadducts formed upon the visible light irradiation are metastable and susceptible to [2+2] cycloreversion due to the significant ring strain of a substituted CB moiety. $^{35-37}$ CB \rightarrow STP reversion is achieved either by UV irradiation at 340 nm or thermal activation, which releases the energy difference between the thermodynamically stable STP and metastable-state CB, $\Delta H_{\text{storage}}$, in the form of heat. Conversely, other CB structures formed by the [2+2] cycloaddition of cinnamates, coumarins, and maleimides undergo cycloreversion by UV irradiation at wavelengths below 300 nm. ³⁸⁻⁴⁰ Furthermore, it is remarkable to observe a thermally induced cycloreversion of CB, a Woodward-Hoffmann forbidden process, performed at a low onset temperature (e.g., 71°C) in the STP/CB system. This is in sharp contrast to the cycloadducts of stilbenes⁴¹ and stilbazoles⁴² that do not thermally cleave upon heating near 200°C and other CBs that undergo thermolysis at temperatures above 400°C. 43 We hypothesize that such facile cycloreversion of CB is achieved due to the unique donor-acceptor structure of STP/CB bearing a cationic acceptor. Specifically, the [2+2] transition state is presumed to be stabilized by the strong donor and acceptor groups, which lower the energy barrier for thermal reversion and also allow for the quantitative analysis of $\Delta H_{storage}$ by differential scanning calorimetry (DSC) of the CB \rightarrow STP process.

In order to investigate the structural parameters that enable the [2+2] cycloaddition of STP and successful energy storage in CB, we have developed a series of compounds with varied counter-anions including BF_4^- , CIO_4^- , Br^- , and $CF_3SO_3^-$ (1–4) and electron-donating groups on the phenyl ring (5–10) (Figure 1C; Schemes S1



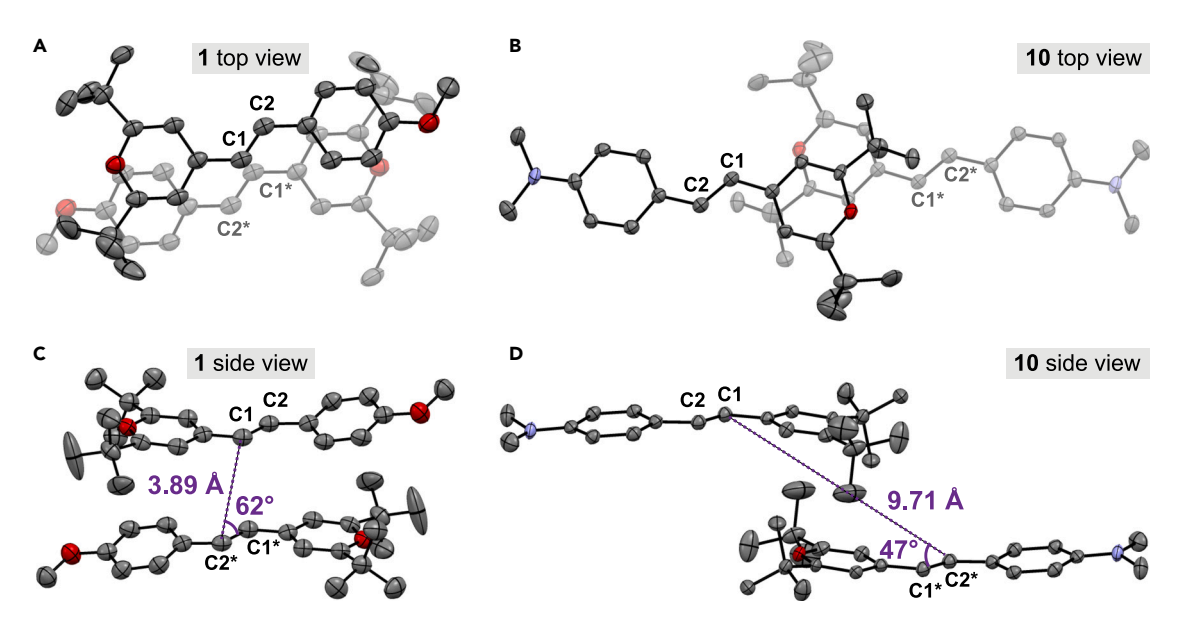


Figure 2. Single crystal structures of STPs 1 and 10 thermal ellipse plots of two crystallographically equivalent and adjacent
(A) STP-1 showing head-to-tail packing and (B) STP-10 showing offset packing. The side views of (C) STP-1 and (D) STP-10 showing C1–C2* distance and C1–C2*–C1* angle measurements. Thermal ellipsoids were set at 50% probability. Hydrogen atoms and BF₄⁻ anions were omitted for clarity.

and S2; Figures S1-S18). Four counter-anions were selected based on the following two criteria: first, the pKa of their conjugate acid should be sufficiently low (below zero) to prevent any nucleophilic side reaction with STPs. Thus, nucleophilic anions including alkoxide and acetate were excluded from the range of viable counter-anions. Second, counter-anions with low molecular weights were chosen to maximize the gravimetric energy density of MOST compounds. Therefore, larger anions such as tosylate and tetrakis(pentaphenylfluoro)borate were excluded from our study. The type (Me, OMe, or NMe₂), number (one, two, or three), and position (ortho, meta, or para) of the electron-donating groups were varied to control the level of electron delocalization over STP structures, which influences both the absorption wavelengths and energy levels of STPs (vide infra). We hypothesized that the packing of cationic compounds and counter-anions in a crystal would determine the energy levels of the STP and CB forms and the energy gap between them. We also postulated that the electronic and steric effects of functional groups would affect the solid-state [2+2] cycloaddition, the E_a of thermal cycloreversion, and the ring strain of CB that may influence $\Delta H_{storage}$. All STP derivatives formed crystalline solids that were irradiated at the peak absorption wavelength of each compound in hexane suspension. STP 1-7 underwent successful cycloaddition at near-quantitative yields (Scheme S3; Figures S19-S30), whereas STP 8-10 did not form CB products even after 48 h of irradiation. In order to unravel the difference, the X-ray diffraction of STP crystals (1, 2, 4-7, 9, 10) was performed to analyze the packing of molecules in solids (Figures 2 and S31-S38; Table S1). Compounds 3 and 8 were unable to form high-quality single crystals for structure analysis.

The crystal structure of STP-1 displays parallel stacking between an electron-rich phenyl and an adjacent electron-deficient pyrylium via π -interactions, forming a head-to-tail pair of two STP molecules (Figure 2A). STPs 2, 4–7, and 9 also exhibit similar head-to-tail packing with different degrees of slippage between the paired molecules (Figure S39). STP-10, on the other hand, shows a different packing structure where two neighboring pyrylium units stack (Figure 2B). The side views of the crystal structures show a clear contrast between the pair of STP-1 and the pair of





Table 1. Pair-overlap parameters and packing structures of STPs 1, 2, 4–7, 9, and 10								
STP	d (C1–C2*) (Å)	<c1-c2*-c1* (°)<="" th=""><th>Packing</th><th colspan="2">Cycloadddition</th></c1-c2*-c1*>	Packing	Cycloadddition				
1	3.89	62	herr.	Υ				
2	3.96	61	herr.	Υ				
4	3.40	75	1D col.	Υ				
5	3.44	73	herr.	Υ				
6	3.90	59	herr.	Υ				
7	4.21	63	1D col.	Υ				
9	4.57	45	herr.	N				
10	9.71	47	1D col.	N				

STPs 3 and 8 were unable to form high-quality single crystals for structure analysis. Viability of cycloaddition: 3 (Y), 8 (N); herr, herringbone pattern; 1D col., 1D columnar pattern.

STP-10. Since the overlap between the neighboring double bonds impacts the success of [2+2] cycloaddition, two structural parameters (i.e., C1–C2* distance and C1–C2*–C1* angle) were chosen to illustrate the degree of overlap. For STP-1, the C1–C2* distance is short (3.96 Å), and the C1–C2*–C1* angle is large (62°), indicating a large degree of overlap between the paired STP molecules (Figure 2C), which allows for facile [2+2] cycloaddition in solid. On the other hand, the C1–C2* distance for STP-10 is significantly longer (9.71 Å), and C1–C2*–C1* angle is smaller (47°) (Figure 2D), representing a large offset between the paired molecules and preventing [2+2] cycloaddition in crystals. STP-10 adopts pseudo-brickwork packing due to the dispersion forces between tBu groups and C–H··· π interactions between tBu and aryl groups (Figure S40).

The crystal structure analysis of STP compounds is summarized in Table 1, revealing the conditions that allow for [2+2] photocycloaddition: the C1-C2* distance up to 4.21 Å and C1-C2*-C1* angle larger than 47°. The overlap between the paired STPs is determined by the functionalization of the phenyl ring. STPs 6-9 possess three electron-donating functional groups (Me or OMe) on the different positions of the phenyl ring; 2, 4, 5-, or 3, 4, 5-functionalized STPs 6 and 7 form a head-totail packed pair with a large overlap and undergo a facile cycloaddition. By contrast, STPs 8 and 9 with a 2, 4, 6-functionalized phenyl ring do not convert to CB because of the unfavorable packing with a large offset. Hirshfeld surface analysis 44 reveals that a counter-anion interacting with two adjacent STPs serves as a staple to form a headto-tail pair with a large overlap (STPs 1, 2, 4, 5, 6, and 7 in Figure S41). H-C=C (olefin) of an STP and H-C (on 2- or 6-position of phenyl) of adjacent STP simultaneously interact with a shared counter-anion. STP-9 with a 2, 4, 6-substituted phenyl ring loses the staple effect, resulting in a larger offset between two STPs, which also translates to the STP-8 structure. Notably, the STP pairs are observed to arrange in two packing patterns (i.e., herringbone or one-dimensional [1D] columnar) (Figures S40 and S42-S50), which is independent of the degree of overlap between paired STPs. For example, the overlap parameters (C1-C2* distance and C1-C2*-C1* angle) of STPs 4 and 5 are similar (Table 1), whereas they adopt different packing patterns in three-dimensional (3D) space. Thus, there is no correlation between the feasibility of photo-induced cycloaddition and the 3D packing structures.

The optical properties of STP/CBs 1–10 were examined in solutions and thin films, as shown in Figures 3A and 3B for 1. CBs in common organic solvents, e.g., dichloromethane or tetrahydrofuran, undergo facile deprotonation; hence, trifluoroacetic acid (TFA) was used to acquire the solution-state absorption spectra of all compounds for both STP and CB states. CBs were first produced in hexane suspensions of STPs under irradiation and then dissolved in TFA. Conjugated STP-1 shows a



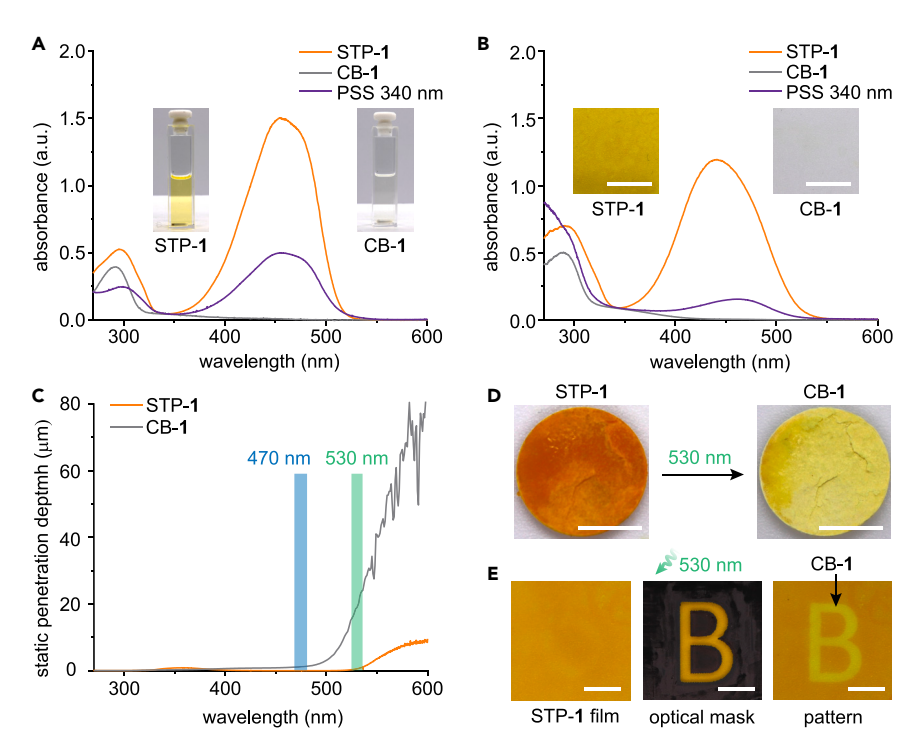


Figure 3. Optical properties of STP/CB-1

(A) UV-vis absorption spectra of STP-1 (orange), CB-1 (gray), and CB-1 at the photostationary state under irradiation at 340 nm with 41% CB \rightarrow STP conversion (purple) obtained in TFA (4 × 10⁻⁵ M for STP-1; 2 × 10⁻⁵ M for CB-1).

(B) UV-vis absorption spectra of STP-1 (orange), CB-1 (gray), and CB-1 at the photostationary state under irradiation at 340 nm with 14% CB \rightarrow STP conversion (purple) measured in 200 nm thin films. Scale bars, 1 cm.

(C) Static light penetration depth calculated for solid-state STP-1 (orange) and CB-1 (gray).

(D) Optical images of STP-1 in a 200 mg pellet (196 μ m thick) before and after the overnight irradiation at 530 nm, yielding 100% cycloaddition. Scale bars, 0.5 cm.

(E) Optical microscope images of an STP-1 film (300 nm) before and after the selective 530 nm irradiation for 15 min through an optical mask, showing a clear pattern formation. Scale bars, 0.5 cm.

strong absorption peak in the range of 400–500 nm, whereas CB-1 displays negligible absorption in the visible light range, confirming the loss of conjugation upon the formation of CB. In addition, the intense first absorption band of STP was observed to red-shift when incorporating a stronger electron donor group: STP-10 (–NMe $_2$) > STP-1 (–OMe) > STP-5 (–Me) (Figure S51). Density functional theory (DFT) calculations attribute this to the increased highest occupied molecular orbital (HOMO) levels and reduced bandgaps of STPs with stronger donor substituents (Figure S52). The photo-induced CB \rightarrow STP cycloreversion was tested in a TFA solution by UV irradiation at 340 nm. Partial reversion was observed by UV-vis spectroscopy, and 41% reversion was quantified by 1 H NMR (Figure S53), which is attributed to the significant overlap between the absorption of STP and CB. The optical properties of other compounds (STPs 2–10 and CBs 2–7) measured in solutions are shown in Figure S54.

Spin-coated thin (200 nm) films of STP and CB show similar absorption features to those obtained in solutions (Figure 3B). The film of STP-1 was irradiated at 470 nm to form 100% CB in 5 h, and partial CB \rightarrow STP cycloreversion was achieved by 340 nm irradiation. Most notably, the film was able to undergo quantitative





 $STP \rightarrow CB$ photocycloaddition using the broad wavelengths of solar light in 12 h, demonstrating the direct harnessing of unfiltered solar irradiation by the STP/CB system (Figures S55 and S58). The solid-state UV-vis absorption spectra of STPs 2-10 and CBs 2-7 are included in Figure S57, and the photocycloaddition kinetics of all STPs under light-emitting diode (LED) and solar irradiation are included in Figures S55 and S56 with the STP → CB conversions confirmed by ¹H NMR (Figures S58-S64). Under irradiation, the spectrum of the STP-8 film did not change, whereas STP-9 and STP-10 underwent decomposition (Figures S65-S67). We note that 470 nm was irradiated on thin films of STPs 1-4 and 6-9, 430 nm on STP-5, and 625 nm on STP-10, depending on their absorption maxima. Although the solar spectrum consists of a broad range of UV and visible light—wavelengths that induce both photocycloaddition and reversion—100% STP → CB conversion was achieved for STPs 1-5 upon 12-h irradiation with a solar simulator (AM 1.5) due to the larger total irradiance of the wavelengths associated with cycloaddition (345-540 nm; 31.3 mW/cm²) compared with reversion (280–344 nm; 4.3 mW/cm²) (Figure S68). Also, inefficient UV-induced CB → STP cycloreversion, observed for all compounds (Figures S53 and S57), contributes to the complete STP \rightarrow CB conversion under broad solar irradiation. We speculate that the slower STP \rightarrow CB process achieved by solar irradiation compared with LEDs is partly attributed to the stronger irradiance levels of LEDs (8.5 mW/cm² at 430 nm; 7.1 mW/cm² at 470 nm) compared with those of solar irradiation (2.8 mW/cm² at 430 nm; 5.7 mW/cm² at 470 nm) at λ_{max} of each STP (Figure S69).

The static light penetration depths of STP-1 and CB-1 (Figure 3C) were calculated based on the measured extinction coefficient of each compound in solutions. It is predicted that the incident light of 470 nm can penetrate through the CB-1 film up to 1 μ m, whereas 530 nm shows a larger penetration depth of 19 μ m, despite the lower absorption of 530 nm by STP-1 (Figure 3B). Therefore, 530 nm was irradiated on a much thicker solid pellet of STP-1 (Figure 3D). Although the irradiance of the 530 nm LED (3.1 mW/cm²) is lower than that of 470 nm (7.1 mW/cm²), the 196 µm-thick sample (Figure S70) was fully converted to CB-1 upon the overnight irradiation at 530 nm, in contrast to the incomplete conversion achieved by 470 nm irradiation (Figure S71). The static light penetration depth refers to the depth of the sample at which the intensity of incident light decays to 1/e. Also, the pressedpowder pellets are not as optically dense as crystals, enabling the complete conversion of samples that are ten times thicker than the theoretical light penetration depth. The photo-induced cycloaddition was further verified by the selective exposure of thin-film STP-1 (300 nm) to 530 nm through an optical mask for 15 min (Figure 3E). The clear contrast between the exposed area that formed CB-1 and the covered area that is intact shows the spatial control over the photocycloaddition and energy storage process, which could be exploited to modulate the total energy storage in a set amount of materials.

The phase and thermal reversion properties of the compounds were monitored by DSC as illustrated in Figures 4A and 4B for compounds 1 and 4. STPs undergo a sharp melting transition upon heating above 200°C then supercool to -90°C without crystallization. The second heating cycle reveals the cold crystallization of the supercooled STPs above 100°C, which is followed by the melting of STPs at T_{m} . The CBs are heated to first undergo CB \rightarrow STP thermal reversion at T_{rev} , releasing the stored energy ($\Delta H_{storage}$), followed by the melting of the restored STPs in a crystalline state. The thermogravimetric analysis (TGA) (Figure S72) and DSC cycles of all compounds are shown in Figures S73–S76, and the NMR spectra of restored STPs after DSC are shown in Figures S77–S83. The photon energy



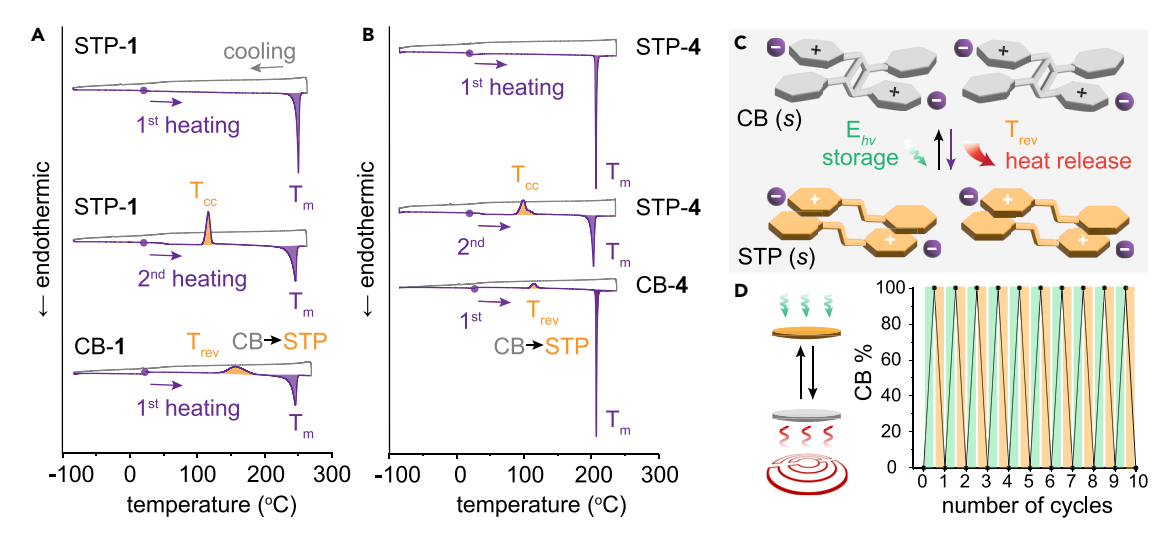


Figure 4. Thermal properties of STPs/CBs 1 and 4

(A) DSC plots of STP-1 during the first two heating and cooling cycles and CB-1 during the first cycle. Purple dots show the initial room temperature at which the heating cycle started.

- (B) DSC plots of STP-4 during the first two heating and cooling cycles and CB-4 during the first cycle.
- (C) Schematic illustration of STP/CB energy storage and release cycle.

(D) Cycling test of compound 1 upon repeated 530 nm irradiation and thermal activation. T_m , melting temperature; T_{cc} , cold crystallization temperature; T_{rev} , thermal reversion temperature.

storage through STP \rightarrow CB and energy release through CB \rightarrow STP achieved at T_{rev} are reversible and repeatable (Figure 4C), and the successful cycling test on a solid pellet of compound 1 (200 mg, 196 μ m thick) was carried out by the repeated overnight 530 nm irradiation and 10-min heating at 160°C (Figure 4D). The solid-state energy storage and release system exhibits excellent thermal and photostability in the absence of any noticeable decomposition over 10 cycles (Figure S84).

We note that T_{rev} and T_{onset} , the peak and onset temperatures of the CB ightarrow STP exotherm, vary across the compounds from 108°C to 180°C (T_{rev}) and from 71°C to 165° C (T_{onset}). The larger values of T_{rev} and T_{onset} generally correlate with the larger activation barriers for thermal reversion (E_a), which is shown in Table 2. The minor inconsistencies result from the different heating conditions used for the DSC measurement of exotherm (heating at 10°C/min) and the solid-state measurement of E_a at constant temperatures (Figure S85). E_a also corresponds to the heat input required for thermally triggered $CB \rightarrow STP$ cycloreversion, and the heat input is recovered while the activated CB at a transition state relaxes to the thermodynamically stable state, generating STP (Figure 1A). Since more energy is released (164 kJ/mol for CB-1) than the heat input (122 kJ/mol for CB-1), the efficiency of energy release is greater than unity, which makes thermal triggering a more effective method than photochemical triggering. UV-induced cycloreversion exhibits very low energy efficiency due to low quantum yields, 45,46 large UV photon energy input, and low solid-state photostationary state (Figure S53). The half-lives of CBs, assessed in the solid state, range from 4 days to 32 years, showing that long-term energy storage is enabled by the molecular design and selection of counter-anions.

The integrated exotherm at T_{rev} , i.e., $\Delta H_{storage}$, also widely varies across the compounds. CBs 1, 2, and 6 display a substantial energy storage density of 37–42 kJ/mol, which is comparable to that of azobenzene (41 kJ/mol). We note that the $\Delta H_{storage}$ value of CB-5 (31 kJ/mol) is underestimated due to the significant





Table 2. CB → STP thermal reversion parameters and 3D packing pattern of each compound										
$CB \rightarrow STP$	T _{rev} (°C)	T _{onset} (°C)	Δ H _{storage} (kJ/mol)	$\Delta H_{storage}$ (J/g)	Packing	E _a (kJ/mol)	τ _{1/2} (days)			
1	157	132	42	51	herr.	122	2,045			
2	155	131	42	49	herr.	121	1,594			
3	142	128	23	28	n.a.	110	18			
4	117	91	8	8	1D col.	113	64			
5	175 ^a	165ª	31 ^a	39 ^a	herr.	126	11,919			
6	108	71	37	42	herr.	106	4			
7	180	154	6	6	1D col.	124	4,830			

 $^{^{}a}T_{rev}$ and T_{onset} are overestimated, and $\Delta H_{storage}$ is underestimated due to the overlap between the CB \rightarrow STP thermal reversion and melting of CB-5; n.a., not available

overlap between the CB → STP thermal reversion and melting of CB-5, which reduces the integrated area of the exotherm (Figure S76E). By contrast, CBs 4 and 7 release markedly less energy during the cycloreversion (6-8 kJ/mol), despite the structural similarity among all compounds. In order to obtain insights into this trend and substitution effect, $\Delta H_{storage}$ of simplified structures 1, 5, 6, 7, and 10 was estimated by DFT calculations, which excludes the consideration of electrostatic interactions (Figures S86 and S87; Table S2). The calculated $\Delta H_{\text{storage}}$ values of the compounds (114 kJ/mol for 6, 112 kJ/mol for 1, 87 kJ/mol for 5, 68 kJ/mol for 7, and 118 kJ/mol for 10) partially agree with the trend obtained from experiments $(\Delta H_{storage} 10 > 1 > 6 > 5 > 7)$. For example, STP-1 (–OMe) reports a larger $\Delta H_{storage}$ than STP-5 (-Me) in both experiment and calculation, which can be rationalized by the larger resonance stabilization of STP-1 compared with STP-5 (Figure S88). However, the deviation of calculated values from those experimentally obtained highlights that not only the relative electronic structures of STP and CB but also intermolecular interactions have a significant effect on $\Delta H_{storage}$. In fact, a strong correlation between the 3D packing pattern and $\Delta H_{storage}$ was discovered—compounds 1, 2, 5, and 6 that display herringbone patterns store larger quantities of energy and compounds 4 and 7 that are packed into a 1D columnar structure store less energy (Table 2). Since the crystal structure of compound 3 could not be obtained, the discussion on 3 is not included.

The drastic effect of 3D packing among compounds on their energy storage capacity was examined by the crystal structure analysis of STP and CB of representative compounds 4 (1D columnar, 8 kJ/mol) and 5 (herringbone, 31 kJ/mol) in Figures 5A and 5B. Due to the difficulty of growing large crystals of CBs, only the crystal structure of CB-4 was newly obtained, and the structure of CB-5 from a crystal structure database was analyzed in comparison.⁴⁷ We hypothesized that (1) structural changes of compounds and (2) displacement of counter-anions in crystals during the [2+2] cycloaddition would influence the relative energy levels of the STP and CB states. First, we observe that the structural changes are more significant for compound 4 in 1D columnar packing during STP -> CB conversion (5% contraction along the b axis) compared with compound 5 in herringbone packing (3% contraction) (Tables S3-S13). However, the overall cell volume change is consistent between compounds 4 and 5 ($V_S/V_C = 1.01$), indicating a slight shrinkage of volume during STP \rightarrow CB for both compounds. Therefore, we investigated the displacement of counter-anions in crystals, which changes the electrostatic interactions among the cationic molecules and counter-ions. The distances between the centroids of STP/CB and three counter-anions around the molecules were measured (d_{S1} , d_{S2} , and d_{S3} for STP and d_{C1} , d_{C2} , and d_{C3} for CB, Figures 5C and 5D). Electrostatic potential maps of compounds 4 and 5 (Figures 5E and 5D) display the delocalized electron deficiency for both STP and CB states, which infers the delocalized electrostatic





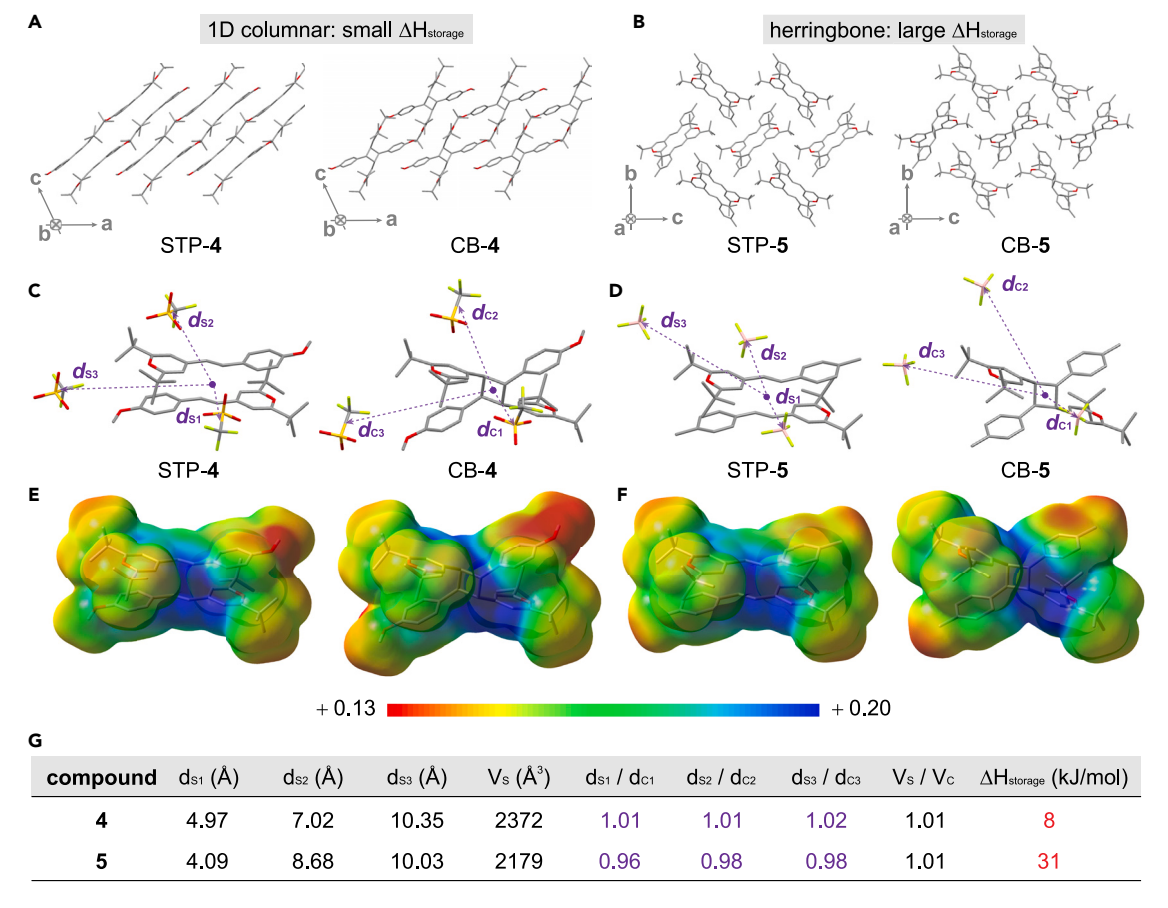


Figure 5. Packing structures of STPs/CBs 4 and 5

(A–F) Crystal packing structures of (A) STP-4 and CB-4 and (B) STP-5 and CB-5, representing 1D columnar and herringbone pattern, respectively. Hydrogen atoms and anions are omitted for clarity. The distance measured between the centroid of compounds (head-to-tail packed STP or CB) and neighboring counter-anions for (C) compound 4 and (D) compound 5. Electrostatic potential map of head-to-tail packed STP or CB for (E) compound 4 and (F) compound 5 calculated at the M062X/6-31+G(d,p) level of theory.

(G) A table summarizing the distance and unit cell volume measured for compounds 4 and 5, the ratio of such values between STP and CB for each compound, and the energy storage density of each compound.

interactions between the anions and the cationic molecules. The ratio $(d_{\rm S}/d_{\rm C})$ was obtained to assess the change in electrostatic interactions during the [2+2] conversion, and $d_{\rm S}/d_{\rm C}$ values smaller than 1 for compound 5 indicate the enhanced Coulombic interaction in the STP form compared with that in the CB state (Figure 5G). Therefore, STP-5 is stabilized, increasing the energy gap between STP-5 and CB-5, hence enhancing $\Delta H_{\rm storage}$. On the contrary, the electrostatic interactions among STP-4 are weaker than those among CB-4, decreasing the energy gap between the two states.

We note that both the [2+2] cycloaddition enthalpy and phase change enthalpy are being captured during the photo-induced solid-to-solid phase transition. In order to quantify the solid-solid phase transition enthalpy, the melting or crystallization enthalpy of STP and CB should be quantified. The melting enthalpy DSC characterization of STPs is shown in Figures S73–S75, whereas that of CBs is unviable for most compounds due to the facile CB \rightarrow STP thermal reversion occurring prior to the melting of CBs (Figure S76). The only exception is CB-5, which exhibits melting before the reversion to STP-5, and the solid-solid phase transition enthalpy (15 J/g) can be estimated by subtracting the melting enthalpy of CB-5 (23 J/g) from

Please cite this article in press as: Cho et al., Solid-state photon energy storage via reversible [2+2] cycloaddition of donor-acceptor styrylpyrylium system, Chem (2023), https://doi.org/10.1016/j.chempr.2023.06.007





that of STP-5 (38 J/g). The ratio between the phase transition enthalpy (15 J/g) and [2+2] cycloaddition enthalpy (39 J/g) is thus estimated as 1:2.6.

This new finding emphasizes the remarkable importance of the 3D packing of STP/CB-based MOST compounds in crystals, which is even more significant than the donor-acceptor strengths or relative positions of functional groups on the compounds. We believe that the cationic nature of STP/CB and the presence of counter-anions result in this unique phenomenon. Specifically, the changes of electrostatic interactions in crystals during photo-cyclization dictate the energy storage capacity of charged MOST compounds. The STP/CB system that shows crystal-to-crystal transitions (Figure S89) and stores energy through intermolecular cycloaddition is unique and sheds light on the utilization of various reported solid-state photochemistry for MOST applications.

Conclusions

We discovered a set of design principles for the STP/CB-based MOST system, including the functionalization patterns on the cationic compounds and the selection of counter-anions, which control the viability of photo-induced [2+2] cyclo-addition in crystals and the relative energy of the STP and CB states. The donor-acceptor type compounds that form head-to-tail packed pairs and arrange into a herringbone pattern in crystals can store up to 42 kJ/mol, which is similar to the energy storage density of azobenzene-based MOST compounds. The energy storage period in the STP/CB system is extremely tunable by molecular designs, ranging from 4 days to 32 years. The new MOST system that absorbs visible light and quantitatively yields metastable CBs in the solid state opens up opportunities to harness the visible light range of solar spectrum and achieve an exclusively solid-state energy device. The development of catalytic or electrocatalytic triggering methods that efficiently release the stored energy is an ongoing effort, which will enable the application of novel materials in large-scale energy devices.

EXPERIMENTAL PROCEDURES

Resource availability

Lead contact

Further information and requests for resources should be directed to and will be fulfilled by the lead contact, Grace G.D. Han (gracehan@brandeis.edu).

Materials availability

Any unique materials generated in this study are available from the lead contact with a completed material transfer agreement.

Data and code availability

Crystallographic data have been deposited in the Cambridge Crystallographic Data Center (CCDC) with the following accession numbers: STP-1 (2241224), STP-2 (2241225), STP-4 (2241204), CB-4 (2241229), STP-6 (2241226), STP-7 (2241227), STP-9 (2241228), and STP-10 (2241289). These data can be obtained free of charge from the CCDC at https://www.ccdc.cam.ac.uk/structures/.

SUPPLEMENTAL INFORMATION

Supplemental information can be found online at https://doi.org/10.1016/j.chempr. 2023.06.007.





ACKNOWLEDGMENTS

This material is based upon work supported by the Air Force Office of Scientific Research under award number FA9550-22-1-0254. G.G.D.H. acknowledges the NSF CAREER award (DMR-2142887) and the Alfred P. Sloan Foundation (FG-2022-18328). S. Cho and X.L. were supported by Brandeis MRSEC (DMR-2011846). We thank Dr. Peter Müller at the MIT Chemistry Department X-Ray Diffraction Facility for the single crystal XRD measurements and the guided analysis of STP-10.

AUTHOR CONTRIBUTIONS

S. Cho synthesized and characterized STPs 1–5, 8, and CBs 1–5; performed ¹H and ¹³C NMR, TGA, and DSC analysis of the compounds; and conducted thin-film photoconversion kinetics experiments. J.U. performed single crystal X-ray structure analysis and interpretation of the results. J.U. provided quantum chemical calculations and contributed to the mechanistic understanding. S. Chakraborty synthesized and characterized STPs 6, 7, 9, and 10 and CBs 6 and 7 and performed ¹H and ¹³C NMR, TGA, and DSC analysis of the compounds. X.L. performed UV-vis absorption spectroscopy, pellet irradiation studies, and powder X-ray diffraction. G.G.D.H. conceived the project, designed the experiments, and refined the manuscript. All authors discussed the results and edited the manuscript.

DECLARATION OF INTERESTS

The authors filed a U.S. provisional application related to this work.

Received: February 28, 2023 Revised: June 10, 2023 Accepted: June 14, 2023 Published: July 11, 2023

REFERENCES

- Shi, Y., Gerkman, M.A., Qiu, Q., Zhang, S., and Han, G.G.D. (2021). Sunlight-activated phase change materials for controlled heat storage and triggered release. J. Mater. Chem. A 9, 9798–9808. https://doi.org/10.1039/ D1TA01007G
- Qiu, Q., Gerkman, M.A., Shi, Y., and Han, G.G.D. (2021). Design of phase-transition molecular solar thermal energy storage compounds: compact molecules with high energy densities. Chem. Commun. (Camb) 57, 9458–9461. https://doi.org/10.1039/ D1CC03742/K
- Shangguan, Z., Sun, W., Zhang, Z.Y., Fang, D., Wang, Z., Wu, S., Deng, C., Huang, X., He, Y., Wang, R., et al. (2022). A rechargeable molecular solar thermal system below 0°C. Chem. Sci. 13, 6950–6958. https://doi.org/10. 1039/D2SC01873J.
- Dong, L., Feng, Y., Wang, L., and Feng, W. (2018). Azobenzene-based solar thermal fuels: design, properties, and applications. Chem. Soc. Rev. 47, 7339–7368. https://doi.org/10. 1039/C8CS00470F.
- Kunz, A., Heindl, A.H., Dreos, A., Wang, Z., Moth-Poulsen, K., Becker, J., and Wegner, H.A. (2019). Intermolecular London dispersion interactions of azobenzene switches for tuning molecular solar thermal energy storage

- systems. ChemPlusChem 84, 1145–1148. https://doi.org/10.1002/cplu.201900330.
- Qiu, Q., Yang, S., Gerkman, M.A., Fu, H., Aprahamian, I., and Han, G.G.D. (2022). Photon energy storage in strained cyclic hydrazones: emerging molecular solar thermal energy storage compounds. J. Am. Chem. Soc. 144, 12627–12631. https://doi.org/10.1021/jacs. 2c05384.
- Orrego-Hernández, J., Dreos, A., and Moth-Poulsen, K. (2020). Engineering of norbornadiene/quadricyclane photoswitches for molecular solar thermal energy storage applications. Acc. Chem. Res. 53, 1478–1487. https://doi.org/10.1021/acs.accounts.0c00235.
- Jorner, K., Dreos, A., Emanuelsson, R., Bakouri, O.E., Galván, I.F., Börjesson, K., Feixas, F., Lindh, R., Zietz, B., Moth-Poulsen, K., et al. (2017). Unraveling factors leading to efficient norbornadiene-quadricyclane molecular solarthermal energy storage systems. J. Mater. Chem. A 5, 12369–12378. https://doi.org/10. 1039/C7TA04259K.
- Brøndsted Nielsen, M.B., Ree, N., Mikkelsen, K.V., and Cacciarini, M. (2020). Tuning the dihydroazulene – vinylheptafulvene couple for storage of solar energy. Russ. Chem. Rev. 89, 573–586. https://doi.org/10.1070/RCR4944.

- Wang, Z., Udmark, J., Börjesson, K., Rodrigues, R., Roffey, A., Abrahamsson, M., Nielsen, M.B., and Moth-Poulsen, K. (2017). Evaluating dihydroazulene/ vinylheptafulvene photoswitches for solar energy storage applications. ChemSusChem 10, 3049–3055. https://doi. org/10.1002/cssc.201700679.
- Wang, Z., Erhart, P., Li, T., Zhang, Z.-Y., Sampedro, D., Hu, Z., Wegner, H.A., Brummel, O., Libuda, J., Nielsen, M.B., et al. (2021). Storing energy with molecular photoisomers. Joule 5, 3116–3136. https://doi.org/10.1016/j. joule.2021.11.001.
- Usuba, J., and Han, G.G.D. (2023). Photoswitch designs for molecular solar thermal energy storage. Trends Chem. https://doi.org/10. 1016/j.trechm.2022.12.010.
- Shao, B., and Aprahamian, I. (2020). Hydrazones as new molecular tools. Chem 6, 2162–2173. https://doi.org/10.1016/j.chempr. 2020.08.007.
- Shao, B., and Aprahamian, I. (2020). Planarization-induced activation wavelength red-shift and thermal half-life acceleration in hydrazone photoswitches. ChemistryOpen 9, 191–194. https://doi.org/10.1002/open. 201900340.

Chem Article



- Klajn, R. (2014). Spiropyran-based dynamic materials. Chem. Soc. Rev. 43, 148–184. https://doi.org/10.1039/C3CS60181A.
- Stricker, F., Sanchez, D.M., Raucci, U., Dolinski, N.D., Zayas, M.S., Meisner, J., Hawker, C.J., Martinez, T.J., and Read de Alaniz, J. (2022). A multi-stage single photochrome system for controlled photoswitching responses. Nat. Chem. 14, 942-948. https://doi.org/10.1038/ s41557-022-00947-8.
- Gonzalez, A., Kengmana, E.S., Fonseca, M.V., and Han, G.G.D. (2020). Solid-state photoswitching molecules: structural design for isomerization in condensed phase. Mater. Today Adv. 6, 100058. https://doi.org/10.1016/ j.mtadv.2020.100058.
- Thaggard, G.C., Haimerl, J., Park, K.C., Lim, J., Fischer, R.A., Maldeni Kankanamalage, B.K.P., Yarbrough, B.J., Wilson, G.R., and Shustova, N.B. (2022). Metal-photoswitch friendship: from photochromic complexes to functional materials. J. Am. Chem. Soc. 144, 23249–23263. https://doi.org/10.1021/jacs.2c09879.
- Griffiths, K., Halcovitch, N.R., and Griffin, J.M. (2022). Efficient solid-state photoswitching of methoxyazobenzene in a metal-organic framework for thermal energy storage. Chem. Sci. 13, 3014–3019. https://doi.org/10.1039/ D2SC00632D.
- Grommet, A.B., Lee, L.M., and Klajn, R. (2020). Molecular photoswitching in confined spaces. Acc. Chem. Res. 53, 2600–2610. https://doi. org/10.1021/acs.accounts.0c00434.
- Gerkman, M.A., Gibson, R.S.L., Calbo, J., Shi, Y., Fuchter, M.J., and Han, G.G.D. (2020). Anylazopyrazoles for long-term thermal energy storage and optically triggered heat release below 0°C. J. Am. Chem. Soc. 142, 8688–8695. https://doi.org/10.1021/jacs.0c00374.
- Gonzalez, A., Odaybat, M., Le, M., Greenfield, J.L., White, A.J.P., Li, X., Fuchter, M.J., and Han, G.G.D. (2022). Photocontrolled energy storage in azobispyrazoles with exceptionally large light penetration depths. J. Am. Chem. Soc. 144, 19430–19436. https://doi.org/10.1021/ jacs.2c07537.
- Li, X., Cho, S., and Han, G.G.D. (2023). Lightresponsive solid-solid phase change materials for photon and thermal energy storage. ACS Mater. Au 3, 37–42. https://doi.org/10.1021/ acsmaterialsau.2c00055.
- Lefebvre, Q., Jentsch, M., and Rueping, M. (2013). Continuous flow photocyclization of stilbenes – scalable synthesis of functionalized phenanthrenes and helicenes. Beilstein J. Org. Chem. 9, 1883–1890. https://doi.org/10.3762/ bioc.9.221.
- Jørgensen, K.B. (2010). Photochemical oxidative cyclisation of stilbenes and stilbenoids-the Mallory-reaction. Molecules

- 15, 4334–4358. https://doi.org/10.3390/molecules15064334.
- Sugiyama, N., Iwata, M., Yoshioka, M., Yamada, K., and Aoyama, H. (1969). Photooxidation of anthracene. Bull. Chem. Soc. Jpn. 42, 1377– 1379. https://doi.org/10.1246/bcsj.42.1377.
- Hesse, K., and Hünig, S. (1985). Mehrstufige reversible redoxsysteme, XLII. [2 + 2]-Photocycloadditionen von α-styrylpyryliumsalzen zu 4,4'-(1,3-cyclobutandiyl)bis(pyrylium)salzen sowie deren thermische und baseninduzierte cycloreversionen. Liebigs Ann. Chem. 1985, 715–739. https://doi.org/10.1002/ JLAC.198519850408.
- Novak, K., Enkelmann, V., Wegner, G., and Wagener, K.B. (1993). Crystallographic study of a single crystal to single crystal photodimerization and its thermal reverse reaction. Angew. Chem. Int. Ed. Engl. 32, 1614– 1616. https://doi.org/10.1002/anie.199316141.
- Corruccini, R.J., and Gilbert, E.C. (1939). The heat of combustion of cis- and transazobenzene. J. Am. Chem. Soc. 61, 2925–2927. https://doi.org/10.1021/ja01265a100.
- Mansø, M., Tebikachew, B.E., Moth-Poulsen, K., and Nielsen, M.B. (2018). Heteroaryl-linked norbornadiene dimers with redshifted absorptions. Org. Biomol. Chem. 16, 5585– 5590. https://doi.org/10.1039/C8OB01470A.
- Tung, C.H., and Guan, J.Q. (1998).
 Regioselectivity in the photocycloaddition of 9-substituted anthracenes incorporated within Nafion membranes. J. Org. Chem. 63, 5857– 5862. https://doi.org/10.1021/jo980412e.
- 32. Suzuki, H. (1952). The spatial configurations and the ultraviolet absorption spectra of the stilbene derivatives. Bull. Chem. Soc. Jpn. 25, 145–150. https://doi.org/10.1246/bcsj.25.145.
- Semenov, A.V., Balakireva, O.I., Tarasova, I.V., Semenova, E.V., and Minaeva, O.V. (2019). Spectroscopic properties of some hydroxylated 2-stilbazole derivatives.
 J. Fluoresc. 29, 1301–1309. https://doi.org/10. 1007/s10895-019-02445-6.
- Beltrán, A., Burguete, M.I., Luis, S.V., and Galindo, F. (2017). Stryrlpyrylium dyes as solvent-sensitive molecules displaying dual fluorescence. Eur. J. Org. Chem. 2017, 4864– 4870. https://doi.org/10.1002/ejoc.201700815.
- Ringer, A.L., and Magers, D.H. (2007). Conventional strain energy in dimethylsubstituted cyclobutane and the gem-dimethyl effect. J. Org. Chem. 72, 2533–2537. https:// doi.org/10.1021/jo0624647.
- Wilson, A., and Goldhamer, D. (1963).
 Cyclobutane chemistry. 1. Structure and strain energy. J. Chem. Educ. 40, 504. https://doi. org/10.1021/ed040p504.

- Dunitz, J.D., and Schomaker, V. (1952). The molecular structure of cyclobutane. J. Chem. Phys. 20, 1703–1707. https://doi.org/10.1063/1. 1700271.
- Bieniek, N., Inacker, S., and Hampp, N. (2021). Cycloreversion performance of coumarin and hetero-coumarin dimers under aerobic conditions: unexpected behavior triggered by UV-A light. Phys. Chem. Chem. Phys. 23, 17703–17712. https://doi.org/10.1039/ D1CP01919H.
- Chesterman, J.P., Hughes, T.C., and Amsden, B.G. (2018). Reversibly photo-crosslinkable aliphatic polycarbonates functionalized with coumarin. Eur. Polym. J. 105, 186–193. https:// doi.org/10.1016/j.eurpolymj.2018.05.038.
- Cardenas-Daw, C., Kroeger, A., Schaertl, W., Froimowicz, P., and Landfester, K. (2012). Reversible photocycloadditions, a powerful tool for tailoring (nano)materials. Macromol. Chem. Phys. 213, 144–156. https://doi.org/10. 1002/macp.201100399.
- Medishetty, R., Bai, Z., Yang, H., Wong, M.W., and Vittal, J.J. (2015). Influence of fluorine substitution on the unusual solid-state [2 + 2] photo-cycloaddition reaction between an olefin and an aromatic ring. Cryst. Growth Des. 15, 4055–4061. https://doi.org/10.1021/acs. cgd.5b00664.
- Schaumann, E., and Ketcham, R. (1982). [2 + 2]-Cycloreversions. Angew. Chem. Int. Ed. Engl. 21, 225–247. https://doi.org/10.1002/anie. 198202253.
- Chanthapally, A., Yang, H., Quah, H.S., Webster, R.D., Schreyer, M.K., Wong, M.W., and Vittal, J.J. (2014). Oxygen-initiated stereoselective thermal isomerisation of a cyclobutane derivative in the solid state. Chemistry 20, 15702–15708. https://doi.org/10. 1002/chem.201405228.
- Spackman, M.A., and Jayatilaka, D. (2009).
 Hirshfeld surface analysis. CrystEngComm 11, 19–32. https://doi.org/10.1039/B818330A.
- Takamuku, S., Beck, G., and Schnabel, W. (1979). Flash photolysis of tetraphenylcyclobutane in solution—a convenient chemical actinometer. J. Photochem. 11, 49–52. https://doi.org/10. 1016/0047-2670(79)85006-6.
- Murata, K., Yoshinari, Yamaguchi, Shizuka, H., and Takamuku, S. (1991). Chemical actinometers in the 250–270 nm region.
 J. Photochem. Photobiol. A 60, 207–214. https://doi.org/10.1016/1010-6030(91)85060-T.
- Lange, R.Z., Hofer, G., Weber, T., and Schlüter, A.D. (2017). A two-dimensional polymer synthesized through topochemical [2 + 2]cycloaddition on the multigram scale. J. Am. Chem. Soc. 139, 2053–2059. https://doi.org/10. 1021/jacs.6b11857.